PHYSICAL REVIEW B **95**, 075157 (2017)

Invisibility cloaking using pseudomagnetic field for photon

Fu Liu,[1] Simon A. R. Horsley,[2] and Jensen Li[1,*]

[1]*School of Physics and Astronomy, University of Birmingham, Birmingham B15 2TT, United Kingdom*

[2]*Department of Physics and Astronomy, University of Exeter, Stocker Road, Exeter EX4 4QL, United Kingdom*

(Received 19 October 2016; published 28 February 2017)

A cylindrical cloak can be interpreted as a controlled mirage upon a transformation from cylindrical to planar stratified layers. Here, we show that such mirage can be obtained using a pseudomagnetic field instead of a gradient index profile, thus enabling an alternative route towards invisibility cloaking. While working equivalently to a conventional cloak, the asymmetry of light bending direction from a pseudomagnetic field enables the cloak to demonstrate an asymmetric transmission property subject to a truncation of the materials near the inner surface of the cloak. Furthermore, such an asymmetry allows us to design transformation optical devices, such as a one-way retroreflector, with asymmetric transmission.

DOI: 10.1103/PhysRevB.95.075157

I. INTRODUCTION

An invisibility cloak, which hinders the detection of an object by an external observer, is an old fantasy shown in many movies and sci-fi novels but has only recently become practical through the introduction of transformation optics (TO) and metamaterials [1–12]. The key feature of an invisibility cloak is that the waves outside the cloak are left undisturbed as if it is just free space, under arbitrary forms of excitations. TO gives an intuitive and flexible way to achieve this by exploiting the form invariance of Maxwell's equations under coordinate transformations. According to the prescription of TO, the light bends inside the cloak due to a gradient refractive index profile (equivalent to the sizes of the dispersion surfaces) and exits the cloak with exactly the same position, direction, amplitude, and phase as if it had passed through free space. On the other hand, the recent developments of materials that act as a pseudogauge field for the electromagnetic field point to a very different way to guide light: through shifting the centers instead of changing the sizes of the local dispersion surfaces. A spatially varying profile of this shifting introduces a pseudomagnetic field that bends light in real space, in a similar fashion to a magnetic field bending electron motion. Such a mechanism in bending light has a very different nature to the usual light bending from an index gradient, leading to a series of unconventional optical phenomena, including one-way photonic edge states, photonic Landau levels, and alternative ways to achieve negative refraction and waveguiding [13–23]. Apart from various existing schemes for realizing such a pseudomagnetic field through the introduction of either spatial or temporal asymmetry into the mutual coupling within an array of resonators, it has been recently shown that such a pseudomagnetic field can be captured simply in terms of effective medium parameters, which can then be realized using metamaterials [24]. It also enables a higher level description and design methodology for designing optical and metamaterial devices. An invisibility cloak is designed here as an example. Due to the very different nature of the light bending mechanism, the pseudomagnetic field breaks the symmetry between the light rays passing through the left and right sides of the object. As we shall see, it makes the cloaking effect asymmetric under a truncation of the materials near the inner radius of the cloak, different from a conventional cloak with the same degree of truncation. As a further example, a retroreflector with one-way propagation property is designed by exploiting the asymmetry introduced by a pseudomagnetic field.

II. INVISIBILITY CLOAK

A. Interpreting invisibility cloak as controlled mirage

A cylindrical cloak in physical space with unprimed cylindrical coordinates (r,φ,z) is shown in Fig. 1(a), with the inner (outer) radius being a (b). It cloaks a cylinder made of perfect electric conductor (PEC) in vacuum. By applying a coordinate transformation

$$y' = y'(r), \quad x' = -b(\varphi - \pi/2), \quad z' = z, \tag{1}$$

the cloak is transformed into horizontally stratified layers in the virtual space with primed Cartesian coordinates (x',y',z'), as shown in Fig. 1(b). Here, we note that the coordinate transformation is only applied on the cloak region $a \leqslant r \leqslant b$ to consider the light ray trajectories entering and exiting the cloak. In principle, the air outside can also be transformed into anisotropic stratified layers in the virtual space. The cylindrical cloak has rotational symmetry so that it works for waves incident from arbitrary directions. After transformation, it implies a translational symmetry in the x' direction. As a result, we only need to consider a finite length in the x' direction, i.e., $-b\pi \leqslant x' < b\pi$, which transforms into a complete circle in physical space.

Under such a coordinate transformation, a cylindrical cloak can be interpreted as a well-controlled mirage. A light ray passing through the cylindrical cloak in the horizontal direction becomes a total-internal reflected ray in the virtual space, as shown by the black arrow trajectories in Fig. 1. The elapsed phase along the ray in the transformed stratified layers should be exactly the same as its counterpart ray elapsed in the cloak in physical space, i.e.,

$$\int k_{y'} dy' + k_{x'} \Delta x' = k_0 \Delta x. \tag{2}$$

*j.li@bham.ac.uk

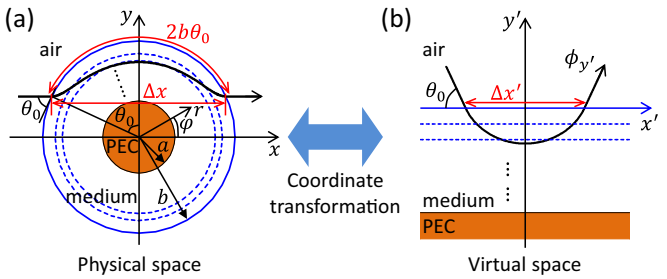

FIG. 1. Transforming a cylindrical cloak in physical space (a) into stratified layers in virtual space (b). The solid (dashed) blue lines illustrating the outer radius (inner rings) of the cloak is (are) mapped to the x' axis (horizontal lines) in virtual space. A ray incident with angle θ_0 experiences curved trajectory and elapses distance Δx in the cloak, as shown by the black arrow line. The corresponding ray in virtual space experiences total-internal reflection with elapsed distance $\Delta x'$. The transformation applies to the cloak region only as we only discuss the light trajectories from entering to exiting the cloak. The air region in the virtual space technically represents an infinitesimal air shell outside the cloak.

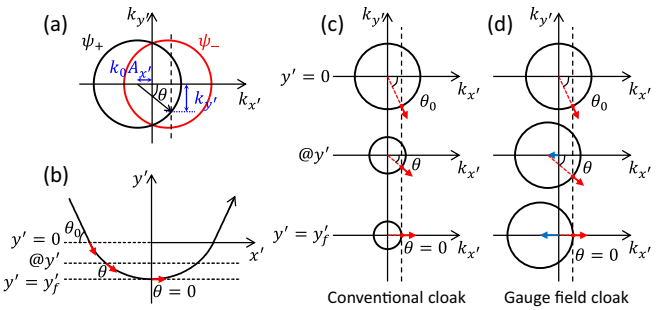

FIG. 2. (a) Dispersion surfaces of the general media described by Eq. (4) at a position where the ray has propagation direction indicated by angle θ in virtual space. The vertical dashed line indicates the momentum matching condition of constant $k_{x'}$. (b) The ray experiences total-internal reflection in the stratified layers in virtual space. At different y' position, the ray has different propagation direction described by angle θ. (c), (d) Two different mechanisms of controlled mirage to achieve the conventional cloak (c) and the cloak with pseudomagnetic field (d).

Here, the total elapsed phase in virtual space is decomposed into two parts. The integration along the ray $\int k_{y'}dy'$ is the phase elapse along the y' direction, where $k_{y'}$ is the wave number in the y' direction. $k_{x'}\Delta x'$ is the phase elapse in the x' direction with $k_{x'}$ being the conserved momentum across the stratified layers and $\Delta x'$ being the elapsed distance in the x' direction. To achieve perfect cloaking, this total elapsed phase must equal the one elapsed through the cylindrical cloak, i.e., $k_0\Delta x$ [see Fig. 1(a)], where k_0 is the wave number in air and Δx is the elapsed distance in the x direction across the cloak. Here we have adopted a ray picture in establishing Eq. (2). We note that it can also be obtained through the WKB approximation, implying that it is accurate for waves except when the wavelength is comparable to the scale of inhomogeneity in the cloak. Equivalently, in the virtual space, the term $\int k_{y'}dy'$ can be interpreted as the reflection phase for a plane wave with incident angle θ_0. Then, a cylindrical cloak can be defined as a black box in the virtual space, with an angular function of reflection phase being specified by Eq. (2), for all incident angles $0 \leqslant \theta_0 < \pi$. We call this the phase condition of the cloak. From the geometry and transformation we know that the angular-dependent elapsed distances are expressed by

$$\Delta x' = 2b\theta_0, \quad \Delta x = 2b\,\sin\theta_0. \tag{3}$$

Next, we discuss the materials in fulfilling the phase condition (2) of the cloak. In this work, we consider general media in virtual space with permittivity and permeability tensors written as

$$\bar{\bar{\epsilon}}' = \begin{pmatrix} 1 & 0 & 0 \\ 0 & 1 & -A_{x'} \\ 0 & -A_{x'} & n'^2 \end{pmatrix}, \quad \bar{\bar{\mu}}' = \begin{pmatrix} 1 & 0 & 0 \\ 0 & 1 & A_{x'} \\ 0 & A_{x'} & n'^2 \end{pmatrix}, \tag{4}$$

where the index n' and anisotropic term $A_{x'}$ are real functions of y'. Such media cover both TO media and media with pseudomagnetic fields. The dispersion surfaces of such media are two circles of decoupled polarizations in the reciprocal space, as shown in Fig. 2(a). The black (red) circle denotes the dispersion of pseudospin-up ψ_+ with $E_z = 1$ and $H_z = 1$ (pseudospin-down ψ_- with $E_z = 1$ and $H_z = -1$). They have the same size of k_0n' and are shifted from the origin with opposite directions by $\mp k_0\boldsymbol{A'}$ where $\boldsymbol{A'} = A_{x'}\hat{x}'$ is the pseudogauge field provided by the above media [24]. A spatially varying $\boldsymbol{A'}$ on the $x'-y'$ plane provides a pseudomagnetic field $\boldsymbol{B'} = \nabla' \times \boldsymbol{A'}$. in the $\hat{z}'$ direction. Such pseudomagnetic field can bend the wave propagation; therefore it can be used to construct an alternative cloak. More details on the metamaterial realization and the associated background of the gauge field can be found in Refs. [24–28]. With these material considerations, we can express the wave numbers inside the medium as

$$k_{x'} = k_0\cos\theta_0, \quad k_{y'} = \mp k_0\sqrt{n'^2 - (A_{x'} + \cos\theta_0)^2}, \tag{5}$$

where $k_{x'}$ is the conserved momentum determined by the incident angle θ_0. The wave number in the y' direction is therefore obtained from the shift dispersion surfaces, as shown in Fig. 2(a). The negative (positive) sign of $k_{y'}$ is chosen before (after) the turning point of the ray propagation in the stratified layers. Then, we can substitute Eq. (5) together with Eq. (3) into Eq. (2) and ask what kinds of material profiles in y' (or equivalently in the r direction) can achieve cloaking for all incident angles in the next section.

For completeness, the material parameters in physical space can be obtained through TO (see Refs. [1–3]) by

$$\begin{aligned} \epsilon_{rr} &= \mu_{rr} = \frac{b}{r}\frac{\partial r}{\partial y'}, \quad \epsilon_{\varphi\varphi} = \mu_{\varphi\varphi} = \frac{r}{b}\frac{\partial y'}{\partial r}, \\ \epsilon_{zz} &= \mu_{zz} = \frac{b}{r}\frac{\partial y'}{\partial r}n'^2, \\ \epsilon_{rz} &= \epsilon_{zr} = -\mu_{rz} = -\mu_{zr} = A_\varphi = -\frac{b}{r}A_{x'}(y'). \end{aligned} \tag{6}$$

It has the same form as conventional transformation optics with decoupled TE/TM polarizations except for the introduction of the nonzero off-diagonal terms, which represent a pseudogauge field in the angular direction $\boldsymbol{A} = A_\varphi\hat{\varphi}$. Again, it gives rise to a pseudomagnetic field by $\boldsymbol{B} = \nabla \times \boldsymbol{A}$.

B. Conventional invisibility cloak

The first possibility in satisfying the phase condition is to use gradient refractive indices n' with $A_{x'} = 0$. In this case, the propagation direction of the ray is modified by the sizes of the dispersion surfaces at different depths, as shown in Fig. 2(c). To realize the total-internal reflection, we need smaller index n' at deeper y' and there is a turning point at which the ray's propagation direction is parallel to x'. This turning point is related to the incident angle θ_0 and for $\theta_0 = \pi/2$ we require $n' = 0$ at the turning point. By solving the phase condition Eq. (2) with Eqs. (3) and (5), we found that the solution is $n'(y') = e^{y'/b}$ in virtual space. It indicates the turning point is at an infinite depth of y' for $\theta_0 = \pi/2$. On the other hand, we can apply the transformation in Eq. (1) to construct a cloak in physical space. As a special case, we choose the radial map as

$$r = be^{y'/b}, \tag{7}$$

which transforms the region $y' \leqslant 0$ into a disk with outer radius $r = b$. The transformed material from Eq. (6) is found being a simple vacuum, which is the starting point of conventional TO. Other kinds of transformation will thus give a conventional cylindrical cloak.

C. Cloaking with pseudomagnetic field

The second possibility is to use the bending nature of pseudomagnetic field originated from a varying $A_{x'}(y')$ while the refractive index is kept constant as $n' = 1$. In this case, the propagation direction of the ray is changed by the shift of the local dispersion surfaces from the gauge field, as shown in Fig. 2(d). And the maximum gauge field required for turning the propagation direction is $A_{x'} = 2$. Because the material has translational symmetry, the ray trajectory is symmetric about y' axis. Therefore, the phase condition Eq. (2) with Eqs. (3) and (5) can be rewritten as

$$\int_0^{y'_f(\theta_0)} \sqrt{1 - (A_{x'} + \cos\theta_0)^2}\, dy' = b(\theta_0 \cos\theta_0 - \sin\theta_0), \tag{8}$$

where $y'_f(\theta_0)$ indicates the lowest position the ray with incident angle θ_0 can reach, i.e., the turning point. The solution can be obtained by expressing y' as a Taylor series of $A_{x'}$:

$$y'_{\text{cloak}}(A_{x'}) = b \sum_{n=1}^{\infty} Y_n \frac{(A_{x'}/2)^n}{n!}, \tag{9}$$

where $Y_n = 8nC_n/(4n^2 - 1) - \sum_{j=1}^{n-1} Y_j C_{n-j}$ with $C_n = -\Gamma_{n-1/2}\Gamma_{n+3/2}/(\pi\Gamma_{n+1})$ and Γ_n is the gamma function. Such Taylor series converges within $0 < A_{x'} \leqslant 2$ and we can use it to numerically approximate the solution. Then the material profile $A_{x'}(y')$ is obtained by its inverse function. Unlike requiring infinite y' in using a refractive index profile, the gauge field proposal only needs a finite depth of y'. As the deepest position corresponds to $A_{x'} = 2$, we can obtain that it is $y'_d = -4.2166b$ (in virtual space) from the solution in Eq. (9). Finally, the material profile in physical space can be obtained through Eq. (6) and we still have the freedom in choosing map $y'(r)$ to construct the invisibility cloak in physical space. Here, as an example, we take a quadratic map

$$y' = \frac{r - b}{b - a}\left(r - a + \alpha b \frac{b - r}{b - a}\right), \tag{10}$$

which transforms $y' = 0$ into the outer boundary of the cloak $r = b$. Such a quadratic map with $dy'/dr = 1$ at $r = b$ ensures the transformed material at $r = b$ is still air, i.e., impedance matched to the outside air to minimize undesired reflection (as we have taken a ray picture). As long as the wavelength is small enough, the impedance is matched in the adiabatic sense to reduce reflection on the outer surface of the cloak. The transformation also maps $y' = -\alpha b$ into the inner boundary of the cloak $r = a$. As the deepest position the rays can reach is y'_d in virtual space, we need $\alpha > 4.2166$ to obtain a cloak that can work for all incident angles. As illustrations, Fig. 3(a) shows the induced material parameters when we choose $a = 1.5$, $b = 4$, and $\alpha = 4.3$. The induced material parameters here are all finite values because of the finite depth required in virtual space. Although they do not diverge into infinity, one of the principal permittivity and permeability (eigenvalues) still become significantly smaller than 1, which requires frequency dispersive metamaterials in realization. Now, the dispersion surfaces in physical space are two shifted ellipses. The size is determined by the indices in radial and angular directions ($n_r = \sqrt{\epsilon_{\varphi\varphi}\epsilon_{zz}}$ and $n_\varphi = \sqrt{\epsilon_{rr}\epsilon_{zz}}$), while the shift is given by the gauge field $\boldsymbol{A} = A_\varphi \hat{\varphi}$ from the off-diagonal values. The bending force in physical space, however, is the combination of the pseudomagnetic field from gauge field $A_\varphi\hat{\varphi}$ and the pseudoelectric field from gradient indices n_r and n_φ.

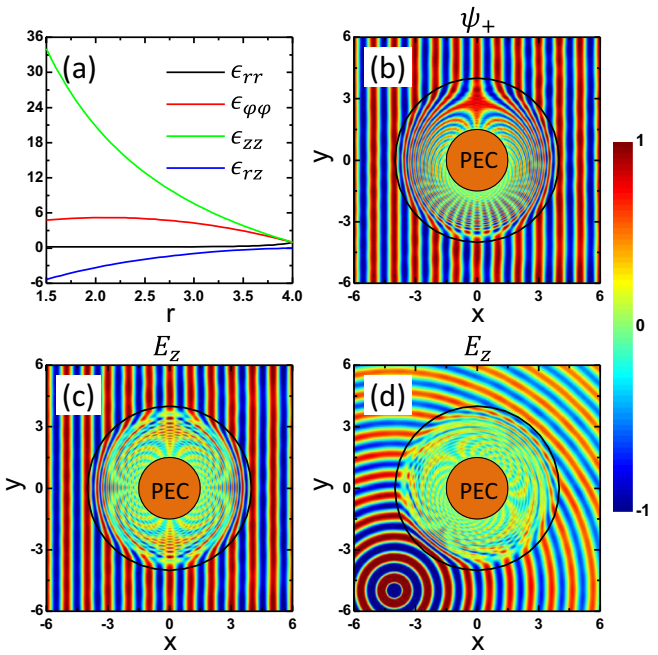

FIG. 3. Invisibility cloak with pseudomagnetic field. (a) Induced material parameters. (b)–(d) Performance of the cloak under ψ_+ (b) E_z (c) plane wave incidence and point source (d) excitation. Working wavelength is $\lambda = 1$. The inner PEC cylinder is cloaked.

The performance of such a cloak enabled by the pseudomagnetic field for photon is illustrated in Fig. 3, from full-wave simulation using COMSOL MULTIPHYSICS (for all simulations

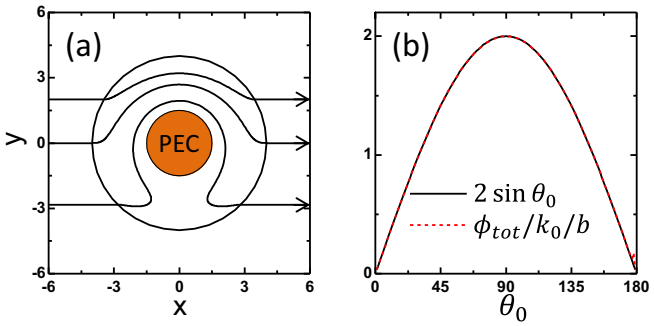

FIG. 4. (a) Trajectories of the rays with incident angles θ_0=60°, 90°, and 135°. (b) Comparison of the measured elapsed phase $\phi_{\rm tot}$ (dashed red line) and the target $2k_0b\sin\theta_0$ (solid black line).

in this work). Figure 3(b) shows the ψ_+ field pattern when a ψ_+ plane wave with wavelength $\lambda = 1$ incident from left. As we can see, the plane wave is transmitted with negligible scattering, making the inner PEC invisible. Inside the cloak, the field is not symmetric about the propagation direction due to the very different bending mechanism in guiding light from one end to the other. The large red spot at the top comes from very small phase velocities $k_\varphi \approx 0$ for waves with incident angle $\theta_0 \approx 90°$. The small features at the bottom are originated from the interference between waves propagating in different directions due to the large incident angles.

We note that once the cloak is designed for pseudospin-up mode, it will automatically work also for pseudospin-down mode as the two pseudospins are time reversal copies of each other. Now if there is a ψ_- plane wave incident from left the ψ_- field pattern inside the cloak is just upside down from that in Fig. 3(b). Therefore, the invisibility cloak can work for any polarization by decomposing it into the two pseudospins. As illustrations, Fig. 3(c) shows the E_z field pattern when there is an E_z (transverse-electric polarization, $\psi_+ + \psi_-$) plane wave incident from left. Moreover, the designed cloak works for any incident direction due to its rotational symmetry and thus works for more arbitrary excitations. Figure 3(d) shows the cloaking effect under an E_z line source excitation. A cylindrical E_z field emitted from a line source located at $(-4, -5)$ still keeps its cylindrical nature after going through the invisibility cloak. In this sense, the cloak employing pseudomagnetic field works equivalently to the conventional cloak, designed by expanding a point into a cylindrical hole [1].

To clearly illustrate how the proposed cloak works, we perform ray tracing [29] for the pseudospin-up mode, as shown in Fig. 4(a). The three arrowed trajectories correspond to three rays with incident angles $\theta_0 = 60°, 90°$, and 135°. As we can see, they are all bent to pass the cloak through the upper part. This is very different from the conventional cloak, in which the rays are bent symmetrically around the PEC core. If there is a small absorption in the designed cloak, it induces a shadow and the shadow becomes asymmetric in the upper and lower parts of the waves exiting the cloak in our case, as the rays entering the lower part of the cloak travel longer and suffer additional loss. On the other hand, the total phase elapsed, $\phi_{\rm tot}$, through the cloak for a ray should satisfy the phase condition Eq. (2), i.e., $k_0 2b\sin\theta_0$ for incident angle θ_0. In Fig. 4(b), we verify this relation by integrating the total phase $\int \boldsymbol{k}\cdot d\boldsymbol{r}$ inside the cloak

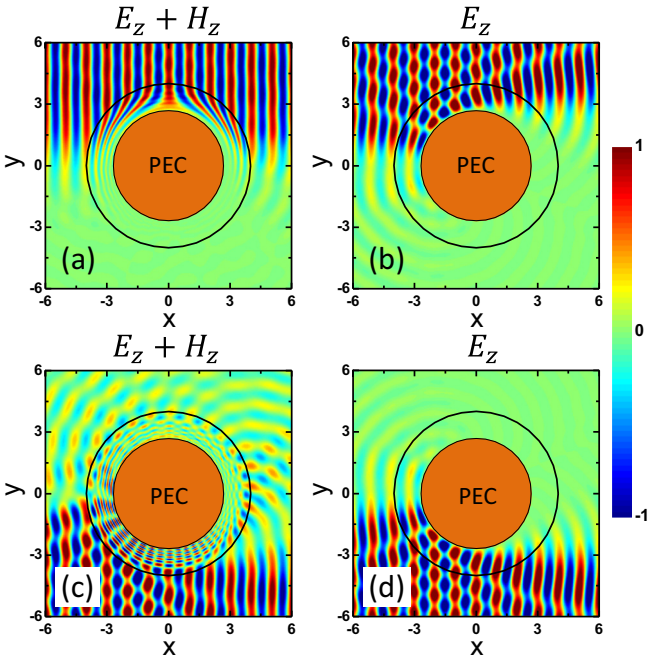

FIG. 5. Performance of the truncated cloaks under upper side excitation [(a), (b)] and lower side excitation [(c), (d)]. (a), (c) Truncated cloak using pseudomagnetic field. (b), (d) Truncated conventional cloak. The truncation means changing the inner material of cloak at $r \leqslant 2.69$ into PEC. Working wavelength is 1.

for each incident angle θ_0, as shown by the red dashed line (normalized by a factor of k_0b). It coincides with the required phase elapse very well.

The cloak proposed here has an advantage that its cloaking functionality is not destroyed if we truncate some inner material to reduce the required anisotropy [see Fig. 3(a)]. The remaining outer device still works for one side incidence, as illustrated in Fig. 5(a). The truncation is performed at $r = 2.69$ mapped from $y' = -1.334$ where $A_{x'} = 1$. The materials inside this position are manually changed into PEC while the outer materials remain. As we can see, when shining a very broad ψ_+ beam which only occupies the upper half space, the truncated cloak still gives very good cloaking performance. However, the same beam entering from the lower half will be scattered completely by the PEC, leaving an obvious shadow, as shown in Fig. 5(c). The scattering occurs similarly, as a form of asymmetric transmission, if the wave runs in the opposite direction for the same spin up in Fig. 5(a). This is because the truncated inner material is only responsible for bending the lower incident waves. This asymmetry for the object lying on the top or bottom side of the incident is introduced through the anticlockwise bending direction of the pseudomagnetic field in virtual space. Furthermore, such a truncated cloak also has unidirectional functionality. While it works for the upper ψ_+ incidence from left as shown in Fig. 5(a), it fails for the upper ψ_+ incident from the right-hand side due to the rotational symmetry of the cloak. These behaviors are very different from its counterpart: a conventional cloak will immediately create a shadow behind it if we truncate the same degree of inner materials, as shown in Figs. 5(b) and 5(d) (designed with the same radii and truncation position as the above cloak

and with a radial map $r = [\frac{a}{b}(\frac{r'}{b} - 2) + 1]r' + a$ [30]). Such a truncation in a conventional cloak is equivalent to introducing a PEC core with radius $r = 2.47$ at the center of virtual space (conventional TO approach). Therefore the shadow is right behind the cloak. From this point of view, the proposed cloak moves the shadow to the lower part for ψ_+ incidence.

III. DESIGN OF RETROREFLECTOR

The design method proposed here by employing the controlled mirage in virtual space also enables us to design other TO devices. As another example, we show that it can also be used to design an omnidirectional retroreflector. A retroreflector, or Eaton lens, is a device that reflects the ray or beam back to the original incident direction for any incident angles [31–33]. We still use the coordinate transformation in Eq. (1) to change the retroreflection into the controlled mirage in virtual space. In this case, the required phase condition is still Eq. (2) but the angular-dependent elapsed distances [original Eq. (3)] are changed to

$$\Delta x' = b(2\theta_0 + \pi), \quad \Delta x = b(2\sin\theta_0 + \pi), \tag{11}$$

where the additional term $b\pi$ means the distance around half the device to realize the retroreflection, as shown in Fig. 6(a). Considering the same gauge field medium with parameters listed in Eq. (4) in virtual space, we can get the phase condition for the retroreflector by substituting Eqs. (11) and (5) into Eq. (2). Similar to the invisibility cloak, the retroreflector also has two kinds of realizations: the conventional one with gradient refractive index and the new one employing the pseudomagnetic field from gauge field metamaterials.

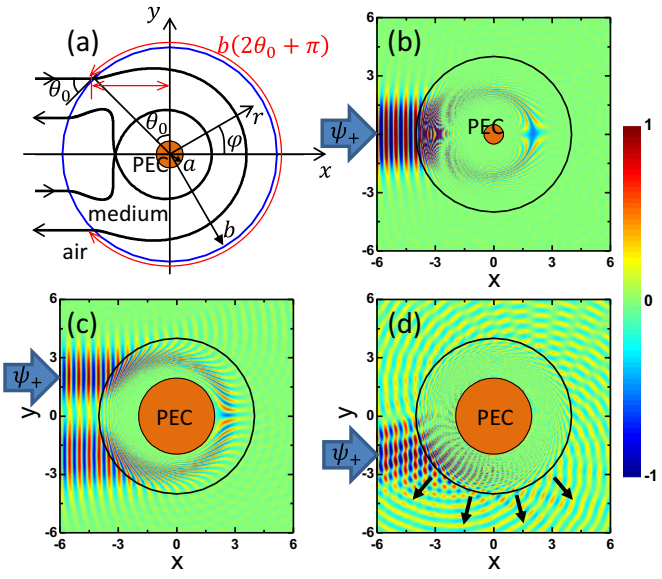

FIG. 6. Retroreflector assisted by pseudomagnetic field. (a) Trajectories of two rays with incident angles $\theta_0 = 45°$ and 110°. The one with larger incident angle experiences a complete circle inside the device. (b) A pseudospin-up beam with wavelength $\lambda = 0.5$ and beam width 4λ incident from the left side will be reflected back to its original route by the retroreflector. (c), (d) Performance of the truncated retroreflector with upper side (c) and lower side (d) beam incidence with wavelength $\lambda = 0.5$ and beam width 4λ.

A. Conventional retroreflector

For the conventional retroreflector (or Eaton lens), we set $A_{x'} = 0$ and only use a gradient profile of refractive index n'. By solving the phase condition, we find that the required index profile in virtual space is $n'(y') = \sqrt{2e^{y'/b} - e^{2y'/b}}$. Then the material parameters in physical space are found to be $\overline{\overline{\epsilon}} = \overline{\overline{\mu}} = \mathrm{diag}\{1, 1, 2b/r - 1\}$ from Eq. (6) if we employ the same coordinate transformation Eq. (1) with radial map Eq. (7). We note that this is the realization of the conventional Eaton lens in two dimensions with refractive indices $n_r = n_\varphi = \sqrt{2b/r - 1}$ and $n_z = 1$ [31–33].

B. Retroreflector using pseudomagnetic field

A retroreflector can also be realized using the gauge field profile $A_{x'}$ which provides a varying pseudomagnetic field for photon. In this case, we set $n' = 1$ and the phase condition for ψ_+ is

$$\int_0^{y'_f(\theta_0)} \sqrt{1 - \left(A_{x'}^2 + \cos\theta_0\right)^2}\, dy' = b[\cos\theta_0(\theta_0 + \pi/2) - \sin\theta_0 - \pi/2]. \tag{12}$$

Comparing with Eq. (8) for cloak, this condition has two more constant terms at the right-hand side. Therefore its solution is the combination of the Taylor series in Eq. (9) for the cloak and another Taylor series responsible for the additional constant terms:

$$y'_{\text{retroreflector}}(A_{x'}) = y'_{\text{cloak}}(A_{x'}) + b\sum_{n=1}^{\infty} \Delta Y_n \frac{(A_{x'}/2)^{n-1/2}}{(n-1/2)!}, \tag{13}$$

where $\Delta Y_n = -\sqrt{\pi}$ for $n = 1$ and $\Delta Y_n = -\sum_{j=1}^{n-1} \Delta Y_j C_{n-j}$ for $n \geqslant 2$. In this case, the deepest position the rays can reach in virtual space is $y'_d = -8.88b$. Then the material profile $A_{x'}(y')$ is obtained again by the inverse function. To construct the retroreflector, we employ the same coordinate map in Eq. (1) with Eq. (10) and the material parameters in physical space are obtained from Eq. (6).

As illustrations, Fig. 6 shows the performance of the designed retroreflector with map parameters $a = 0.5$, $b = 4$, and $\alpha = 9.0$. The larger α here, comparing with the one used in the cloak, is because of the deeper penetration of the waves in virtual space. By using a ray tracing technique, Fig. 6(a) shows the ψ_+ trajectories for two rays coming from left with incident angles $\theta_0 = 45°$ and 110°. As we can see, they are both reflected back to left by the device. Moreover, the ray with $\theta_0 = 110°$ experiences a complete circular route inside the device, which will not happen in the conventional Eaton lens. This comes from the anticlockwise bending nature of pseudomagnetic field in virtual space and the circling can only be in the clockwise direction in physical space. On the other hand, Fig. 6(b) shows the ψ_+ field pattern when a broad ψ_+ beam enters the device from left. The beam is reflected back to where it comes from even if the beam consists of a range of incident angles. We note that this is

an omnidirectional retroreflector as the designed device has rotational symmetry. In addition, similar to a truncation on the cloak, a truncated retroreflector can still work for one side incidence, i.e., asymmetric transmission, as the inner material is only responsible for large incident angles. As illustrations, Figs. 6(c) and 6(d) show the performance of a truncated retroreflector, in which the materials at $r \leqslant 1.95$ ($r = 1.95$ correspond to $A_{x'} = 1$ in virtual space) are manually changed to PEC. When a ψ_+ beam enters from the upper side, it can be reflected back, as shown in Fig. 6(c). However, when the same beam enters from the lower part, it will be scattered because its path is blocked by the replaced PEC, as shown in Fig. 6(d). We note that due to the time reversal symmetry between the two pseudospins, this retroreflector designed for ψ_+ will automatically work for ψ_- and similar behaviors hold. By recognizing the cloak and retroreflector are 0 and 180° propagation direction rotators, the scheme proposed here can be extended to design arbitrary rotators, such as a 90° rotator to bend the propagation direction by 90°.

IV. CONCLUSION

We have explored how transformation optical devices can be designed with pseudomagnetic fields, which can be mimicked by using anisotropic metamaterials. Due to the very different nature of the light bending mechanism, the pseudomagnetic field introduces an asymmetry to a cloak between the light rays passing through the left and right sides of the object. It makes a cylindrical cloak with pseudomagnetic field have asymmetric transmission behavior under a truncation of the materials near the inner surface of the cloak. It also allows us to demonstrate an omnidirectional retroreflector with asymmetric transmission activated by a truncation of the materials at inner radii.

ACKNOWLEDGMENT

This work is supported by the European Union's Seventh Framework Programme under Grant Agreement No. 630979 (NHermPhoton).

[1] J. B. Pendry, D. Schurig, and D. R. Smith, Science **312**, 1780 (2006).
[2] U. Leonhardt, Science **312**, 1777 (2006).
[3] D. Schurig, J. J. Mock, B. J. Justice, S. A. Cummer, J. B. Pendry, A. F. Starr, and D. R. Smith, Science **314**, 977 (2006).
[4] H. Chen, Z. Liang, P. Yao, X. Jiang, H. Ma, and C. T. Chan, Phys. Rev. B **76**, 241104(R) (2007).
[5] R. Liu, C. Ji, J. J. Mock, J. Y. Chin, T. J. Cui, and D. R. Smith, Science **323**, 366 (2009).
[6] J. Valentine, J. Li, T. Zentgraf, G. Bartal, and X. Zhang, Nat. Mater. **8**, 568 (2009).
[7] X. Chen, Y. Luo, J. Zhang, K. Jiang, J. B. Pendry, and S. Zhang, Nat. Commun. **2**, 176 (2011).
[8] J. Zhang, L. Liu, Y. Luo, S. Zhang, and N. A. Mortensen, Opt. Express **19**, 8625 (2011).
[9] M. Gharghi, C. Gladden, T. Zentgraf, Y. Liu, X. Yin, J. Valentine, and X. Zhang, Nano Lett. **11**, 2825 (2011).
[10] J. Hao, Y. Yuan, L. Ran, T. Jiang, J. A. Kong, C. T. Chan, and L. Zhou, Phys. Rev. Lett. **99**, 063908 (2007).
[11] I. I. Smolyaninov, V. N. Smolyaninova, A. V. Kildishev, and V. M. Shalaev, Phys. Rev. Lett. **102**, 213901 (2009).
[12] X. Ni, Z. J. Wong, M. Mrejen, Y. Wang, and X. Zhang, Science **349**, 1310 (2015).
[13] M. Hafezi, E. A. Demler, M. D. Lukin, and J. M. Taylor, Nat. Phys. **7**, 907 (2011).
[14] R. O. Umucalılar and I. Carusotto, Phys. Rev. A **84**, 043804 (2011).
[15] M. Hafezi, S. Mittal, J. Fan, A. Migdall, and J. M. Taylor, Nat. Photon. **7**, 1001 (2013).
[16] K. Fang, Z. Yu, and S. Fan, Phys. Rev. Lett. **108**, 153901 (2012).
[17] K. Fang, Z. Yu, and S. Fan, Nat. Photon. **6**, 782 (2012).
[18] M. C. Rechtsman, J. M. Zeuner, Y. Plotnik, Y. Lumer, D. Podolsky, F. Dreisow, S. Nolte, M. Segev, and A. Szameit, Nature (London) **496**, 196 (2013).
[19] L. D. Tzuang, K. Fang, P. Nussenzveig, S. Fan, and M. Lipson, Nat. Photon. **8**, 701 (2014).
[20] K. Fang and S. Fan, Phys. Rev. Lett. **111**, 203901 (2013).
[21] Q. Lin and S. Fan, Phys. Rev. X **4**, 031031 (2014).
[22] M. C. Rechtsman, J. M. Zeuner, A. Tünnermann, S. Nolte, M. Segev, and A. Szameit, Nat. Photon. **7**, 153 (2013).
[23] F. de Juan, J. L. Mañes, and M. A. H. Vozmediano, Phys. Rev. B **87**, 165131 (2013).
[24] F. Liu and J. Li, Phys. Rev. Lett. **114**, 103902 (2015).
[25] F. Liu, Z. Liang, and J. Li, Phys. Rev. Lett. **111**, 033901 (2013).
[26] F. Liu, S. Wang, S. Xiao, Z. H. Hang, and J. Li, Appl. Phys. Lett. **107**, 241106 (2015).
[27] S. A. Tretyakov, I. S. Nefedov, and P. Alitalo, New J. Phys. **10**, 115028 (2008).
[28] I. V. Lindell and L. H. Ruotanen, J. Electromagn. Waves Appl. **12**, 1131 (1998).
[29] D. Schurig, J. B. Pendry, and D. R. Smith, Opt. Express **14**, 9794 (2006).
[30] W. Cai, U. K. Chettiar, A. V. Kildishev, V. M. Shalaev, and G. W. Milton, Appl. Phys. Lett. **91**, 111105 (2007).
[31] J. E. Eaton, Naval Research Laboratory Report No. 4110, 1953.
[32] J. H. Hannay and T. M. Haeusser, J. Mod. Opt. **40**, 1437 (1993).
[33] Y. G. Ma, C. K. Ong, T. Tyc, and U. Leonhardt, Nat. Mater. **8**, 639 (2009).